PNAS

Main Manuscript for

Proteasome inhibitor bortezomib stabilizes and activates p53 in hematopoietic stem/progenitors and double negative T cells *in vivo*

Yuezhen Xue[1], Boris San Luis[1], Regine Dress[2], Katzrin Binte Ahmad Murad[1], Florent Ginhoux[2-4], Nick Barker[1, 5*], David Lane[1, 6*]

[1]Institute of Molecular and Cell Biology (IMCB), Agency for Science, Technology and Research (A*STAR), Singapore 138648, Singapore.

[2]Singapore Immunology Network (SIgN), A*STAR, Singapore 138648, Singapore.

[3]Department of Immunology and Microbiology, Shanghai Institute of Immunology, Shanghai Jiao Tong University School of Medicine, Shanghai 200025, China

[4]Translational Immunology Institute, SingHealth Duke-NUS Academic Medical Centre, Singapore 169856, Singapore

[5]Department of Physiology, Yong Loo Lin School of Medicine, National University of Singapore, Singapore 117593, Singapore.

[6]Department of Microbiology, Tumor and Cell Biology, Karolinska Institutet, Stockholm, 171 77, Sweden

*Nick Barker

Email: nicholas_barker@imcb.a-star.edu.sg

*David P. Lane

Email: dplane@imcb.a-star.edu.sg

Author Contributions: XY designed and supervised the project; performed experiments and analyzed data; wrote the manuscript. BSL performed experiments, analyzed data, and wrote the manuscript. RD performed experiments, analyzed data and edited the manuscript. KBAM performed experiments. FG designed the project and interpreted data. NB and DL designed and supervised the project, wrote and edited the manuscript.

Competing Interest Statement: The authors declare no competing interests.

Classification: BIOLOGICAL SCIENCES and Cell Biology.

Key Words: p53, hematopoietic stem and progenitor cells (HSPCs), bortezomib, apoptosis

This PDF file includes:

Main Text
Figures 1 to 5

Note: Supporting information in a separated file

Abstract

We have previously shown that proteasome inhibitor bortezomib stabilizes p53 in stem and progenitor cells within gastrointestinal tissues. Here, we characterize the effect of bortezomib treatment on primary and secondary lymphoid tissues in mice. We find that bortezomib stabilized p53 in significant fractions of hematopoietic stem and progenitor cells in the bone marrow, including common lymphoid and myeloid progenitors, granulocyte-monocyte progenitors and dendritic cell progenitors. Stabilization of p53 is also observed in multipotent progenitors and hematopoietic stem cells, albeit at lower frequencies. In the thymus, bortezomib stabilizes p53 in $CD4^{-}CD8^{-}$ T cells. Although there is less p53 stabilization in secondary lymphoid organs, cells in the germinal centre of the spleen and Peyer's patch accumulate p53 in response to bortezomib. Bortezomib induces the upregulation of p53 target genes and p53 dependent/independent apoptosis in the bone marrow and thymus, suggesting that cells in these organs are robustly affected by proteasome inhibition. Comparative analysis of cell percentages in the bone marrow indicates expanded stem and multipotent progenitor pools in p53 p53R172H mutant mice compared with p53 wild-type mice, suggesting a critical role for p53 in regulating the development and maturation of hematopoietic cells in the bone marrow. We propose that progenitors along the hematopoietic differentiation pathway express relatively high levels of p53 protein, which under steady-state conditions is constantly degraded by Mdm2 E3 ligase; however, these cells rapidly respond to stress to regulate stem cell renewal and consequently maintain the genomic integrity of hematopoietic stem/progenitor cell populations.

Significance Statement

p53 stabilization occurs specifically in hematopoietic stem and progenitor cells (HSPCs), double negative T cells and B cell blasts in response to proteasome inhibitor bortezomib that visualizes p53 in healthy hematopoietic and lymphatic tissues without genotoxic reagents. However, excess levels of p53 expression might be harmful to normal tissues. This new understanding of p53 induction by bortezomib in hematopoietic and lymphatic cells is expected to guide rational synergistic combinations by combining the drug with other p53 activators and immunomodulating drugs. Our findings also reveal possible p53 immune functions and its application in cancer immunotherapy.

Introduction

Hematopoiesis is initiated from a rare population of multipotent hematopoietic stem cells (HSCs) that can self-renew and differentiate into all blood lineages (1). HSCs produce multipotent progenitor cells (MPPs) that further differentiate into lymphoid-primed multipotent progenitors (LMPPs) and the progenitors of two main categories of leukocytes - common myeloid progenitors (CMPs) for myelopoiesis and common lymphocyte progenitors (CLPs) for lymphopoiesis according to the classic hierarchical tree-like model of hematopoiesis (2). HSCs also produce immediate progenitors of erythrocytes and platelets called megakaryocyte/erythroid progenitors (MEPs). Hematopoietic progenitor cells (HPCs) are immature cells that ultimately differentiate into all mature blood cells via a fast-amplifying process. The development of immune cells from hematopoietic stem and progenitor cells (HSPCs) is a complex process, and their maturation involves the bone marrow, circulation, residing tissues, pathogen interactions, etc. Granulocyte-macrophage progenitors (GMPs) derive from CMPs and produce 4 types of granulocytes that play critical roles in the innate immune system; the most abundant granulocytes are neutrophils. Macrophages are produced by differentiation of monocytes within tissues. Monocytes and dendritic cells (DCs) are tissue-resident immune cells that rapidly mature upon encountering a pathogen. Their immediate progenitors in the bone marrow are macrophage-dendritic progenitors (MDPs) and common dendritic progenitors (CDPs). B lymphocytes remain in the bone marrow for maturation. In contrast, the progenitors of T lymphocytes exit the bone marrow and migrate to and colonize the thymus, undergoing a series of maturation steps before terminal differentiation.

The entire process of hematopoiesis is subjected to multiple checkpoint regulation and cell death mechanisms (3, 4). The role of p53 in regulating hematopoietic pathways has become evident from studies using genetically engineered mice, in which either loss or mutation of p53 itself or p53 pathway components led to aberrant immune profiles and increased incidence of leukemia and lymphoma (5, 6). The p53 pathway, activated in response to DNA damage in eliminating stressed, damaged, or otherwise suboptimal cells for tissue function and homeostasis, is well established (7). Genomic stresses such as radiation exposure or genotoxic agents activate the serine/threonine kinases ataxia-telangiectasia mutated kinase, which stabilize p53 and induce the upregulation of p53 target genes, resulting in cell cycle arrest and/or apoptosis. Mutant p53 can also be stabilized but lacks normal p53's

tumor suppression function and has potentially gained oncogene properties (8). The critical roles of p53 in cell cycle processes and thus cell proliferation have been well established (9-11). Recent studies have identified a role for p53 in the maintenance of quiescence in HSCs and in cell cycle checkpoint regulation of hematopoietic cells (12). Little is known about the involvement of p53 pathways in hematopoiesis and particularly in progenitor cell populations that have high cell plasticity and might be prone to tumorigenesis under stress or following gene mutation.

Proteasome inhibitor bortezomib is a modified dipeptidyl boronic acid and an inhibitor of the proteasomal degradation machinery, aiding the stabilization of proteins/substrates (13). We previously characterized the effects of bortezomib in stabilizing and activating p53 in proliferative compartments of mouse gastrointestinal organs (14). We also noted stabilization of p53 in cell fractions within hematopoietic organs. It is essential to explore the effects of bortezomib on normal hematopoietic cells since it is the first proteasome inhibitor anticancer drug used in treating multiple myeloma and mantle cell lymphoma (15). Here, we expanded our initial observations and identified the cell populations that had stabilized p53 within lymphoid tissues in response to bortezomib, particularly in the bone marrow and thymus, the primary site of hematopoiesis and T cell development. We further analyzed the immune compartments of p53-mutant mice to address the impact of p53 itself in HSC, progenitor, and mature immune cell populations.

Results

Rapid induction of p53 in a subset of bone marrow cells in response to bortezomib

p53 roles in immune cell differentiation and replenishment of tissue immune cells from the bone marrow HSC pool is poorly understood. We addressed the kinetics of p53 stabilization induced by bortezomib treatment in the bone marrow. Mice were injected intraperitoneally with bortezomib at 3 mg/kg and examined at 0.5 hour (h), 1.5h, 3h, 6h, 9h, 18h, 24h, 48h, and 72h compared to vehicle control (Ctrl as BTZ 0h) (Fig. 1*A*). The vertebra and femur/tibia were harvested for bone marrow p53 IHC analyses. In bone marrow, p53 stabilization by bortezomib was induced throughout the course of 0.5-6h (Fig. 1*B*, 1*C*), after which p53 expression gradually returned to basal levels by 24h post treatment. Peak p53 staining intensities were observed 1.5h post-bortezomib treatment. The kinetics of bortezomib-induced p53 stabilization observed here for the bone marrow differed from our previous observations in gastrointestinal organs (14). Significant levels of p53 stabilization were maintained for up to 6h after treatment in cell populations within bone marrow, whereas gastrointestinal organs typically displayed p53 stabilization for only 1.5h. Basal p53 levels are readily detectable in mouse bone marrow (Fig. 1*C*, purple arrows, Fig. 1*B*, light brown), indicating relatively high level expression of p53 protein despite its active degradation. The rapid increase of p53 protein in response to bortezomib in the bone marrow further indicates that a large amount of protein is continuously synthesized but actively degraded. Such a mechanism is likely to facilitate rapid activation of p53 in response to endogenous/exogenous stress signals to protect hematopoietic cells from genotoxic injury.

Bortezomib stabilizes p53 in stem and progenitor cells of the bone marrow

To determine the cell populations stabilized for p53 in response to bortezomib in the bone marrow, we designed flow cytometry staining panels for hematopoietic stem/progenitors, as well as fully mature immune cells (*SI Appendix*, Table S1), and employed various gating strategies for HSPCs, myeloid and lymphoid cells based on immune markers (*SI Appendix*, Fig. S1*A*-*C*). We harvested the bone marrow at 1.5h post-bortezomib treatment, when the highest levels of p53 expression were present. 5-10% of HSCs ($Lin^-Sca\text{-}1^+c\text{-}Kit^+CD135^-$) displayed p53 stabilization following bortezomib treatment (Fig. 2*A*, 2*A'*). Increased frequencies of $p53^+$ cells were found in multipotent progenitor cells MPPs and LMPPs, and frequencies increased still further in early progenitors such as CLP, GMP, CMP, MEP, and MDP (19-60%). In contrast, the frequency of $p53^+$ cells were reduced in intermediate progenitors (CDPs) and further reduced to basal levels in precursors and various mature hematopoietic cells (Fig. 2*A'*, 2*B*, *SI Appendix*, Fig. S1*D*). For example, MDPs, which are dendritic cell (DC) early progenitors, showed significantly elevated frequencies of $p53^+$ cells comparable to intermediate progenitors (CDPs) after bortezomib treatment (Fig. 2*B*). The frequency of $p53^+$ cells was at basal levels in DC precursors (pre-DCs). Most mature immune cells such as cDC, pDC and monocytes, neutrophils, and T cells in the bone marrow present lower frequencies of $p53^+$ cells following bortezomib treatment, except ~ 1% of B cells and ~ 6% of NK cells (Fig. 2*A'*, 2*B*).

In summary, we examined the stabilization of p53 in 18 cell types, including HPSCs and mature hematopoietic cells, representing 75% of the $CD45^+$ cells in the bone marrow (Fig. 2*C*, *SI Appendix*,

Table S2). Under normal conditions (Fig. 2*D*, vehicle control mice), p53 was observed in only 0.004% of CD45$^+$ cells, including HSC, CMP, MEP and tissue-resident cells cDC, pDC and Mono cells. In BTZ-treated mice (Fig. 2*E*), 0.85% of CD45$^+$ cells were positive for p53, and the dominant p53$^+$ cells in the bone marrow were GMP, CMP, MEP, B cells and NK cells. *Trp53* transcripts were detected in the bone marrow and colocalized with *Kit*, a cytokine receptor expressed in HSCs and multiple hematopoietic progenitors (Fig. 2*F*). High levels of *Trp53* transcripts and rapid stabilization of p53 in HSPCs of the bone marrow in response to proteasome inhibition, suggesting robust levels of p53 transcription and translation within this compartment and potential p53 roles in maintaining genomic integrity in hematopoietic stem and progenitor cell populations.

Bortezomib drives p53 activation and p53 mutation leads to the expansion of hematopoietic stem/progenitor cell pool in bone marrow

To determine if bortezomib-stabilized p53 is functionally active and whether p53-dependent cellular effects are induced in response to bortezomib in the bone marrow, we performed quantitative PCR (qPCR) analysis on bone marrow samples from p53wt and p53ko mice injected with 3 mg/kg bortezomib or vehicle control for 3h rather than 1.5h time point to capture p53 target gene response following p53 protein stabilization (Fig. 3*A*, 3h). We detected maximum p53 stabilization at 1.5h after bortezomib treatment (Fig. 1*B*-*C*). However, we found that p53 target genes were mostly induced after 3h (or longer) of bortezomib treatment. Specifically, we analyzed p53 target genes known to be involved in cell cycle arrest (*Cdkn1a*/p21), apoptosis (*Bbc3*/Puma), and DNA repair (*Gadd45a*). To estimate the p53-specific effects on cell cycle-relevant genes, we also quantified mRNA levels of *Ccna2.* In bone marrow, bortezomib-induced p53 stabilization resulted in upregulation of *Cdkn1*a and *Bbc3* (Fig. 3*B*). In contrast, the cell cycle genes *Ccna2*, DNA repair gene *Gadd45a*, and mRNA levels of *Trp53* itself were unaffected by p53 stabilization at these time points. Protein induction of p21 and Puma, detected by IHC at 3h and 9h post bortezomib treatment, was readily apparent in p53wt mice (Fig. 3*C*, 3*D*). In contrast, there was no detectable upregulation of cell cycle arrest and pro-apoptotic genes in the bone marrow of p53-knockout mice treated with bortezomib. These results demonstrate that bortezomib-induced stabilization of p53 is crucial for the upregulation of downstream genes involved in cell cycle arrest and apoptosis.

We measured bortezomib-induced apoptosis in the bone marrow of p53wt and p53ko mice by analyzing expression of cleaved caspase 3 at the indicated time points (Fig. 3*A*, 3*E*). We detected a significant increase in the frequency of cleaved caspase 3$^+$ cells as early as 3h post-bortezomib administration in p53wt mice. Apoptosis was also consistently induced at 6h, 9h, and 18h post-bortezomib administration, albeit at decreasing frequencies (Fig. 3*E*, 3*E'*). In contrast, apoptosis in the bone marrow of p53ko mice was only observed at 9h post-bortezomib administration, indicating the existence of a p53-independent apoptotic cascade in the bortezomib-treated bone marrow. These findings demonstrate that bortezomib treatment stabilizes transcriptionally active p53 to drive activation of p53 target genes and p53-dependent apoptosis, highlighting important p53-mediated regulatory activities in response to bortezomib within the hematopoietic stem and progenitor cells of the bone marrow.

Robust stabilization of p53 by BTZ and its target gene induction in the bone marrow prompted us to explore whether p53 mutation would affect hematopoiesis and immune cell differentiation. We compared the frequency of different cell types in the bone marrow of 5-6m p53$^{+/+}$ (p53wt) and p53$^{R172H/R172H}$ (p53mt) mice. p53R172H is known for losing p53 transcriptional function and p53mt mice are tumor prone and get sick when they age. Increased frequencies of HSC, MPP, and LMPP were observed in p53mt mice (Fig. 3*F*). The frequencies of all downstream progenitors and mature cells were not significantly changed in p53mt mice compared with p53wt mice, suggesting that p53 mutation has less impact on lineage commitment progenitors and mature cells. Collectively, we found a noticeable increase in stem and early progenitor frequencies in the bone marrow of p53mt mice, especially in HSC and MPP, which comprise the bone marrow stem cell pool (3) and serve as the primary source of cells that reconstitute all blood lineages through hematopoiesis. These findings indicate an important role for p53 in maintaining and regulating differentiation of immune cell stem/progenitor cells in the bone marrow.

Bortezomib treatment stabilizes p53 in double negative T cells in the thymus

We next sought to determine how p53 is stabilized by bortezomib in the thymus, another primary lymphoid organ specific for T cell development and maturation. IHC analyses of p53 expression in the thymus revealed a significant number of cells that stabilized p53 upon bortezomib treatment. p53 stabilization was induced throughout the course of 0.5-24h treatment, predominantly within the cortex region (Fig. 4*A*, *SI Appendix*, Fig. S2*A*) where T cell precursors undergo cell division and commence

TCR gene arrangements. p53 expression levels peaked at 3h and stayed high for 9h. p53 expression returned to basal levels at much later time points, 48/72h post bortezomib administration in the thymus rather than 24h in the bone marrow (Fig. 4*A*, *SI Appendix*, Fig. S2*A*, 1*C*), indicating variations in cell turnover rates, drug metabolism or p53 degradation mechanisms in different organs.

T cell progenitors migrate from the bone marrow to the thymus and then differentiate via $CD4^-CD8^-$ (double negative, DN) to $CD4^+CD8^+$ (double positive, DP) thymocytes, and finally to either CD4 or CD8 single positive (SP) T cells (16). Thus, we analyzed these four $CD4^{+/-}CD8^{+/-}$ subpopulations using flow cytometry analyses (Fig. 4*B*). Although DP cells are the dominant cell population in the thymus (*SI Appendix*, Fig. S2*B*), expression levels of p53 were particularly high in DN thymocytes, the earliest stage of differentiation, compared to all other populations; ~42% of DN thymocytes stabilized p53 in response to bortezomib (Fig. 4*C* left panel, 4*C'*). In contrast, only 1-5% of DP and SP thymocytes presented stabilized p53 and no p53 stabilization was observed in vehicle controls. The DN population can be subdivided into four subsets, based on expression of the surface proteins CD44 and CD25: $CD44^+CD25^-$ (DN1), $CD44^+CD25^+$ (DN2), $CD44^-CD25^+$ (DN3) and $CD44^-CD25^-$ (DN4) (Fig. 4*B*). Numerous gene rearrangements such as αβTCR rearrangement occur during transition from DN3 to the DN4 cell population. 25 - 75% of DN2, DN3, and DN4 subsets stabilized p53, and DN4 exhibited the highest p53 levels after bortezomib treatment (Fig. 4*C* right panel, 4*C''*). The DN1 subset failed to stabilize p53. p53 was thus prominently stabilized in DN thymocytes that represent the earliest T cell precursors in the thymus, while p53 levels decreased with further differentiation into DP and SP thymocytes.

Bortezomib treatment also upregulated expression of *Cdkn1a* and *Bbc3* in the thymus (Fig. 4*D*). As observed in the bone marrow, no significant changes in expression of *Gadd45a*, *Trp53*, and *Ccna2* in response to bortezomib occurred in the thymus. In contrast to the mode of apoptosis-induction in the bone marrow, two waves of apoptosis occurred in the thymus in response to bortezomib, the first peak at 1.5-3h and the second peak at 18/24h post administration (Fig. 4*E*, *SI Appendix*, Fig. S2*C*). Although p53-dependent apoptosis was observed at 3h post bortezomib treatment, apoptosis was also induced in the thymus of p53ko mice at both 3h and 18/24h, albeit rather at low levels, suggesting that thymocytes are more sensitive to proteasome inhibition. Strikingly, DN and DP thymocytes were perturbed by p53 mutation with increased frequencies of DN and reduced frequencies of DP in p53mt mice (Figure 4*F*). There appears to be a stall up in the DP stage in the p53mt mice; malfunction of p53 in the transition from the DN stage to the DP stage could be the reason that leads to abnormal cell maturation and ultimately lead to tumorigenesis.

Bortezomib treatment stabilizes p53 in secondary lymphoid tissues and blood

The spleen and lymph node are two major secondary lymphoid organs that host mature lymphoid and myeloid populations, especially B cells, T cells and DCs, which coordinate to serve their immune functions by generating immune responses and tolerance. Therefore, we focused on mature lymphoid and myeloid cell populations in these two organs. In contrast to the bone marrow and thymus, we observed far fewer p53-stabilized cells in the spleen (*SI Appendix* Fig. S3*A*) except for clusters of germinal centre cells (Fig. 5*A*, red arrows). $p53^+$ cells were scattered throughout the red pulp, white pulp, and marginal zones of the spleen (Fig. 5*A*). Several immune cell subsets exhibited bortezomib-induced p53 stabilization, albeit at much lower frequencies than p53 stabilization in HSPCs, but comparable to the same cell types in bone marrow. The frequency of p53 stabilization in B cells, NK cells, and $CD4^+$ or $CD8^+$ T cells in the spleen is 0.8-1.2%. In the myeloid population, 4.9% of conventional DC1 (cDC1) displayed stabilized p53 (Fig. 5*B*, 5*B'*, *SI Appendix*, Fig. S3*B*, S3*C*). In summary, we detected 64% of the total $CD45^+$ cell population in the spleen, comprising mainly B and T cells (Fig. 5*C*, *SI Appendix*, Table S3). In control mice, p53 was spontaneously expressed in a small percentage of cells, including NK cells and $CD4^+$ and $CD8^+$ T cells (Fig. 5*D*, left panel, ΔCtrl. Δ = $p53^+$ frequency - $isotype^+$ frequencies). In bortezomib-treated mice, the major p53-stabilized populations were B cells, $CD4^+$ and $CD8^+$ T cells, and a small percentage of NK cells and DCs (Fig. 5*D*, right panel, ΔBTZ).

The frequency of p53-stabilized cells induced by bortezomib in the mesenteric lymph node (mLN) was comparable to the results observed in the spleen, with higher fractions of NK cells presenting p53 stabilization than in the spleen (Fig. 5*E*, 5*E'*, *SI Appendix*, Fig. S3*D*). Notably, 9.8% of macrophages had stabilized p53 after bortezomib treatment in the mLNs, but not in the spleen and bone marrow (*SI Appendix*, Fig. S3*C*). In the mLN, we detected 87% of the total $CD45^+$ cell population, comprising mainly B and T cells (Fig. 5*F*, *SI Appendix*, Table S4). p53 was spontaneously expressed in a small percentage of cells identified as $CD4^+/CD8^+$ T cells, dendritic cells, and NK cells in control mice (Fig. 5*G*, left panel). In bortezomib-treated mice, the major p53 stabilized populations were still B cells and $CD4^+/CD8^+$ T

cells (Fig. 5*G*, right panel), but the frequencies of $CD4^+$/$CD8^+$ T cells were higher in the mLN than in the spleen, indicating distinct p53 immune functions in the mLN and spleen. We also observed a striking bortezomib-driven stabilization of p53 in the geminal centre of the Peyer's patch (*SI Appendix*, Fig. S4*A*), where rapidly proliferating B cell blasts undergoing somatic hypermutation and IgV gene rearrangement reside (17). p53 stabilization peaked at 1.5h and 3h post-bortezomib treatment. p53-dependent apoptosis occurred at 3-6h, whilst p53-independent apoptosis occurred at 9h post bortezomib treatment (*SI Appendix*, Fig. S4*B*). There was no significant increase in the frequencies of p53 stabilization in detected cell types in the blood in response to bortezomib (*SI Appendix*, Fig. S5*A*, S5*A'*). We detected 77% of the total $CD45^+$ cell population in the blood (*SI Appendix*, Fig. S5*B*), p53 stabilization was observed in low percentages of neutrophils, B cells, and NK cells in control mice, and in low percentages of B cells, $CD4^+$ and $CD8^+$ T cells in BTZ treated mice in the blood (*SI Appendix*, Fig. S5*C*). Collectively, our analyses of p53 stabilization in different secondary and tissue-associated lymphoid structures reveal several immune cell populations with the capacity to stabilize p53 upon proteasomal inhibition with bortezomib to various extents that may reflect their specific p53 immune functions.

Discussion

Few studies have elucidated the expression and/or activity of p53 in hematopoietic tissues in the absence of DNA damage or outside the context of hematologic malignancies. Without using genotoxic reagents, we performed proteasomal inhibition using the drug bortezomib that stabilizes and visualizes wild-type p53 protein and employed immunophenotypic profiling to identify specific myeloid and lymphoid progenitor subsets in mouse bone marrow and $CD4^-CD8^-$ DN cells in the thymus where p53 protein translation is activated in healthy tissues. After administering a single manufacturer-recommended dose (1.3 mg/m^2) of bortezomib to patients (18), an initial plasma distribution half-life is less than 10 minutes, maximum proteasome inhibition happens in 1 hour and final elimination half-life more than 40 hours, returns to baseline around 72-96 hours. p53 stabilization by bortezomib in various lymphatic organs of mice was induced throughout the course of 0.5-6h and gradually returned to basal levels by 24h or 48/72h post treatment, which coincide with the dynamic distribution and half-life of bortezomib in humans. In addition, we observed robust *Trp53* transcripts in HSCs and multiple hematopoietic progenitor populations. Our findings are in consistent with recently published single-cell transcriptomics data in mice, revealing high *Trp53* transcription levels in bone marrow progenitors, DN thymocytes and immature T cells in the thymus (19). This tempts us to speculate that p53 is stabilized by bortezomib in cells that highly transcript p53 mRNA and the stabilization of p53 protein reaches its peak protein levels during the maximum proteasome inhibition period. The presence of robust p53 mRNA levels in the immune stem/progenitor cells and those cells prompt respond to bortezomib indicates an intrinsic ability to initiate rapid p53 protein translation, achieve increased levels of p53 protein, and ensure immediate responses to exogenous or endogenous stresses to maintain the genomic integrity of hematopoietic stem/progenitor cell populations.

Although there is less p53 stabilization in secondary lymphoid organs, cells in the germinal centre of the spleen and Peyer's patch accumulate p53 in response to bortezomib. Several immune cell populations in the spleen and lymph node with the capacity to stabilize p53 upon proteasomal inhibition to various extents that may reflect their specific p53 immune functions. In response to bortezomib treatment, 1) extremely high levels/frequencies of p53 stabilization were detected in proliferating B cell blasts in the germinal centres of the spleen and Peyer's patch, indicating a possible role for p53 in gene rearrangement and somatic hypermutation 2) Higher frequencies of p53 stabilization in $CD4^+$ and $CD8^+$ T cells of the spleen and mLN compared with bone marrow, revealing T cell function in secondary lymphoid organs in helping T cell-dependent antigen to activate B cells. 3) Higher frequencies of p53 stabilization in cDC1 and cDC2 antigen-presenting cells involved in T cell activation in the spleen and mLN. 4) Markedly higher frequencies of p53 stabilization in macrophages of the mLN, an important population that engulfs and digests pathogens, including cancer cells. Whilst we have previously established p53 roles in regulating the M2 polarization process (21), the observed capacity of many other immune populations to stabilize p53 suggests other, currently unknown functions of p53 in the immune system. Excess levels of p53 may be harmful to normal proliferative tissues, especially bortezomib treatment induces hematopoietic symptoms in patients – thrombocytopenia which is highly correlated with an altered NF-κB pathway (22). However, the effect of stabilized p53 on hematopoietic symptoms during bortezomib treatment needs to be evaluated. More investigation is needed to develop novel methods to improve the benefits of p53 activation in cancer therapy and to reduce its side effects.

As we have previously observed in the small intestine (14), bortezomib treatment upregulates the expression of p53 target genes associated with cell cycle arrest (*Cdkn1a*/p21) and apoptosis (*Bbc3*/Puma) in both the bone marrow and thymus, demonstrating that in a significant fraction of bone marrow progenitors and thymocyte DN subsets, p53 protein is activated and maintained, potentially poised to trigger cell-cycle arrest or apoptosis. In turn, this may limit the size of the bone marrow stem and progenitor pool. In developing T and B cells, we found that the highest p53 stabilized populations are in the $CD4^{-}CD8^{-}$ DN T cell subset and in activated B cells forming the germinal centre, both of which undergo VDJ recombination or expansion upon successful pre-TCR or pre-BCR gene rearrangement (16, 17, 23). Consistent with this notion, we and others found that 5-6m p53mt or p53ko mice become sick or develop tumors in different organs, most frequently in hematopoietic organs and especially in thymus (24-26). Transcriptional inactivation of p53 led to increased frequencies of stem and progenitor populations, most notably HSPs and MPPs (Fig. 5*F*). The phenotypes resulting from loss of p53 function are most prominent in the thymus with markedly increased the frequency of DN and reduced DP cell populations. Loss of p53 function by point mutation or gene deletion in these cell populations would lead to aberrant proliferation and differentiation, promoting tumorigenesis in these organs. We are interested in exploring whether the cell populations in the thymus displaying bortezomib-driven p53 stabilization contribute to the development of lymphomas, the most prevalent tumour type that occurs in p53mt and p53ko mice.

Materials and Methods

Mice and bortezomib treatment: C57BL/6 mice were used in this study. All experiments and procedures were approved by the A*STAR Institutional Animal Care and Use Committee (IACUC) and performed in compliance with IACUC regulations. Experiments generally used male mice ranging from 8 to 12 weeks old, except in comparisons between p53 wild-type and p53R172H strains (8), in which mice were also used at 5-6 months of age. Bortezomib (S1013) was purchased from Selleck Chemicals and dissolved in DMSO at 5 mg/ml stock concentrations. The drug was diluted in PBS and injected intraperitoneally at 3 mg/kg.

Immunohistochemistry (IHC), *in situ* hybridization (ISH) and imaging: IHC was performed as described previously (8). Harvested tissues were fixed in cold 10% natural buffered formalin (NBF) for 36-40 hours and sent to histopathology facility (Advanced Molecular Pathology lab, AMPL) for paraffin block embedding. Tissues were sectioned at 5 µm sections and deparaffinized for IHC. The most critical step for p53, p21 and Puma IHC staining is that we used EDTA based pH 9.0 antigen retrieval solution to exposure antigen epitopes. The details of antibodies used for IHC see *SI Appendix*, Table S5. The quantification of p53+ and cleaved caspase 3^{+} populations was calculated by counting immune-positive cells in 20x magnification images. Duplex mRNA ISH was performed according to the manufacturer's instructions using a RNAscope 2.5 duplex Assay and *Trp53* and *Kit* probes (ACDbio). FFPE blocks prepared for IHC can be used for ISH, however, tissue sections need to be freshly prepared. Slides were imaged using Nikon microscope with NIS-Elements software.

Flow cytometry: Staining Panels (*SI Appendix*, Table S1): Panel 1 for hematopoietic stem and progenitor cells; Panel 2 for myeloid cells; Panel 3 for lymphocytes; and Panel 3 modified for the analysis of double-negative T cell subsets in the thymus. Reagents used for flow cytometry are listed in *SI Appendix*, Table S5. Antibodies against specific cell surface markers are listed in *SI Appendix*, Table S6 (Antibody list). Preparation and staining of cells from bone marrow, spleen, thymus, lymph nodes and peripheral blood were performed as previously described (27). Cocktails for cell surface marker staining used antibodies for flow cytometry at a concentration of 1:100 in FACS buffer. For staining panels that include biotinylated antibodies, samples were incubated with streptavidin-conjugated PE-Cy7 (1:300 in FACS buffer) for 15 min in the dark at 4 °C. For intracellular staining of p53, cells were fixed and permeabilized for 20 min at RT using eBioscience Fix/Perm reagents (Thermofisher). Samples were then stained with either anti-p53 or IgG isotype control in the dark at 4 °C for 45 min (1:200 in FACS buffer) and resuspended in FACS buffer for acquisition on an LSRII instrument (BD Biosciences). Data were analyzed using FlowJo software (Tree Star).

Real-time quantitative RT-PCR: Bone marrow samples isolated from femurs and tibias were treated with RBC lysis buffer (Roche) and stored in TRIzol reagent. Thymic lobes were homogenized in TRIzol using TissueLyser LT equipment (Qiagen). Total RNA was prepared using RNeasy mini kit (Qiagen) following manufacturer's protocols and cDNA synthesized using iScript Reverse Transcription Supermix (Bio-Rad). Real-time qPCR was performed using SYBR Green Supermix (Bio-Rad). Primers used are listed in *SI Appendix*, Table S7.

Statistical analysis: All statistical analyses were performed using GraphPad Prism 8.1.2 (GraphPad Software, Inc.). Two-way ANOVA was used for multiple comparisons and paired *t*-test for comparisons between groups.

Acknowledgments

We thank Ashok Venkitaraman and his team, He Ping Ping, and Teena Thakur in Disease Intervention Technology Lab (DITL) for resource and technical support. We thank the Advanced Molecular Pathology laboratory (AMPL) and the flow cytometry platform at Singapore Immunology Network. This work was funded by the Agency for Science, Technology and Research (A*STAR) of Singapore. NB is also supported by National Research Foundation Investigatorship (Award no. NRF12017-03).

References

1. S. H. Orkin, L. I. Zon, Hematopoiesis: an evolving paradigm for stem cell biology. *Cell* **132**, 631-644 (2008).
2. S. E. W. Jacobsen, C. Nerlov, Haematopoiesis in the era of advanced single-cell technologies. *Nat Cell Biol* **21**, 2-8 (2019).
3. E. Laurenti, B. Gottgens, From haematopoietic stem cells to complex differentiation landscapes. *Nature* **553**, 418-426 (2018).
4. T. Chavakis, I. Mitroulis, G. Hajishengallis, Hematopoietic progenitor cells as integrative hubs for adaptation to and fine-tuning of inflammation. *Nat Immunol* **20**, 802-811 (2019).
5. V. Pant, A. Quintas-Cardama, G. Lozano, The p53 pathway in hematopoiesis: lessons from mouse models, implications for humans. *Blood* **120**, 5118-5127 (2012).
6. L. A. Donehower, G. Lozano, 20 years studying p53 functions in genetically engineered mice. *Nat Rev Cancer* **9**, 831-841 (2009).
7. A. J. Levine, p53, the cellular gatekeeper for growth and division. *Cell* **88**, 323-331 (1997).
8. A. M. Goh *et al.*, Mutant p53 accumulates in cycling and proliferating cells in the normal tissues of p53 R172H mutant mice. *Oncotarget* **6**, 17968-17980 (2015).
9. K. Engeland, Cell cycle arrest through indirect transcriptional repression by p53: I have a DREAM. *Cell Death Differ* **25**, 114-132 (2018).
10. M. E. Perry, A. J. Levine, Tumor-suppressor p53 and the cell cycle. *Curr Opin Genet Dev* **3**, 50-54 (1993).
11. A. Hafner, M. L. Bulyk, A. Jambhekar, G. Lahav, The multiple mechanisms that regulate p53 activity and cell fate. *Nat Rev Mol Cell Biol* **20**, 199-210 (2019).
12. Y. Liu *et al.*, p53 regulates hematopoietic stem cell quiescence. *Cell Stem Cell* **4**, 37-48 (2009).
13. J. Adams, M. Kauffman, Development of the proteasome inhibitor Velcade (Bortezomib). *Cancer Invest* **22**, 304-311 (2004).
14. Y. Xue *et al.*, Bortezomib Stabilizes and Activates p53 in Proliferative Compartments of Both Normal and Tumor Tissues In Vivo. *Cancer Res* **79**, 3595-3607 (2019).
15. G. K. Dy *et al.*, A phase I and pharmacologic trial of two schedules of the proteasome inhibitor, PS-341 (bortezomib, velcade), in patients with advanced cancer. *Clin Cancer Res* **11**, 3410-3416 (2005).
16. M. Mingueneau *et al.*, The transcriptional landscape of alphabeta T cell differentiation. *Nat Immunol* **14**, 619-632 (2013).
17. N. S. De Silva, U. Klein, Dynamics of B cells in germinal centres. *Nat Rev Immunol* **15**, 137-148 (2015).
18. E. Hafter, [Meteorism]. *Schweiz Med Wochenschr* **98**, 1049-1051 (1968).
19. C. Tabula Muris *et al.*, Single-cell transcriptomics of 20 mouse organs creates a Tabula Muris. *Nature* **562**, 367-372 (2018).

20. S. Nestorowa *et al.*, A single-cell resolution map of mouse hematopoietic stem and progenitor cell differentiation. *Blood* **128**, e20-31 (2016).
21. L. Li *et al.*, A unique role for p53 in the regulation of M2 macrophage polarization. *Cell Death Differ* **22**, 1081-1093 (2015).
22. S. Lonial *et al.*, Risk factors and kinetics of thrombocytopenia associated with bortezomib for relapsed, refractory multiple myeloma. *Blood* **106**, 3777-3784 (2005).
23. J. P. de Villartay, V(D)J recombination deficiencies. *Adv Exp Med Biol* **650**, 46-58 (2009).
24. W. Hanel *et al.*, Two hot spot mutant p53 mouse models display differential gain of function in tumorigenesis. *Cell Death Differ* **20**, 898-909 (2013).
25. K. P. Olive *et al.*, Mutant p53 gain of function in two mouse models of Li-Fraumeni syndrome. *Cell* **119**, 847-860 (2004).
26. C. Dudgeon *et al.*, The evolution of thymic lymphomas in p53 knockout mice. *Genes Dev* **28**, 2613-2620 (2014).
27. A. Cossarizza *et al.*, Guidelines for the use of flow cytometry and cell sorting in immunological studies (second edition). *Eur J Immunol* **49**, 1457-1973 (2019).

Figures and Figure Legends

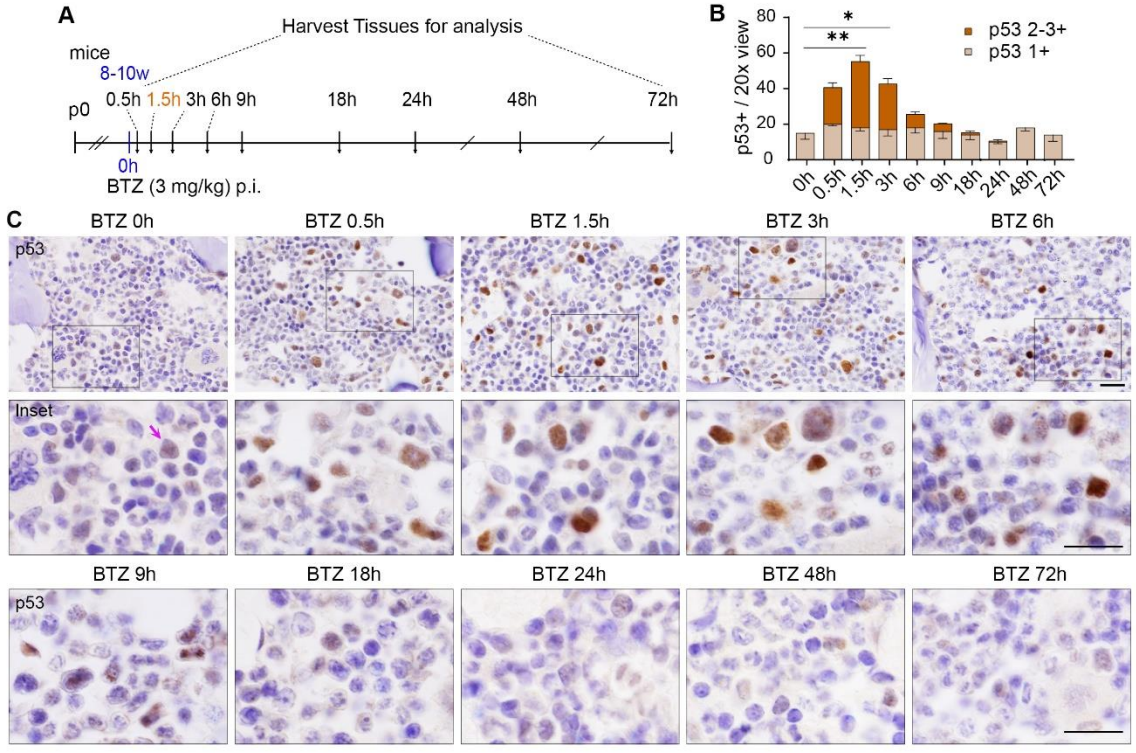

Fig. 1. Time course for the stabilization of p53 by bortezomib in mouse bone marrow. (*A*) The schedule of bortezomib (BTZ) time course experiments (n = 3-4). p0, neonatal; w, week, h, hour; p.i., intraperitoneal injection. (*B*) Quantification of p53-positive frequencies at various time points from mice treated with vehicle (BTZ 0h) or BTZ. Moderate and strong p53 staining signals are classified as p53 2-3+ (in brown), mild p53 staining signals are classified as p53 1+ (in light brown). The indicated *p* values were calculated by multiple unpaired t-tests using Prism. *, $P < 0.05$; **, $P < 0.001$. Error bars represent the Mean (SEM) for each group. (*C*) IHC analysis of p53 in bone marrow from mice at indicated time points post 3 mg/kg BTZ treatment. Purple arrow points to detectable p53 in cells treated with vehicle, indicating high p53 activity in the bone marrow. Scale bars, 20 μm.

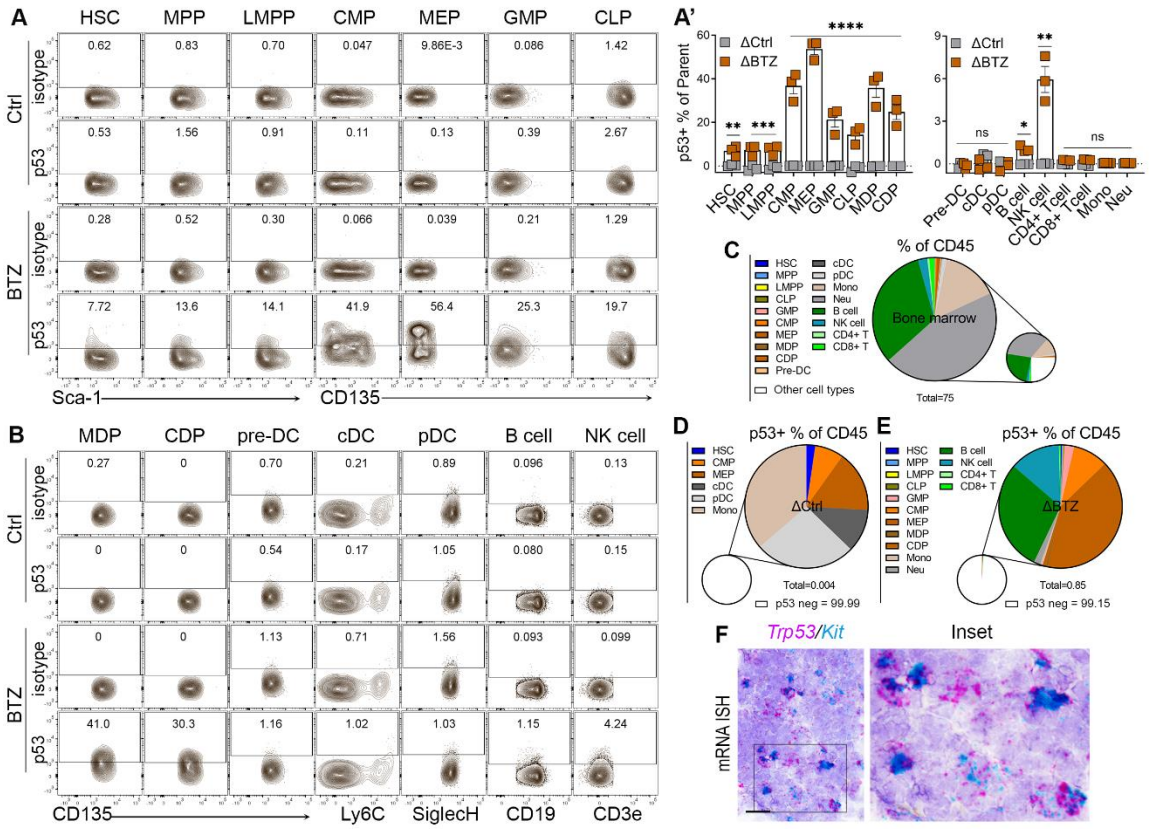

Fig. 2. Stabilization of p53 in the HSPCs of mouse bone marrow by bortezomib. (*A*) Representative FACS plots showing bone marrow cells stained for p53 or isotype controls from mice treated with Ctrl or BTZ, gated on different HSPC populations (n = 3-4). (*A'*) Quantification of p53-positive frequencies of HSPCs and mature cells from mice treated with Ctrl (in grey) or BTZ (in red). The indicated *p* values were calculated by multiple unpaired t-tests using Prism. *, $P < 0.05$; **, $P < 0.001$; ***, $P < 0.0001$; ****, $P < 0.0001$; ns, no significance. The error bars represent the Mean (SEM) for each group. (*B*) Representative FACS plots showing the bone marrow cells stained for p53 or isotype control from mice treated with Ctrl or BTZ, gated on DC progenitors/precursors, matured DC and B/NK cells (n = 3-4). (*C*) Quantification of frequencies of various $CD45^+$ HSPCs and mature cells from mice treated with Ctrl only. (*D* & *E*) Quantification of frequencies of $p53^+$ in HSPCs and mature cells of $CD45^+$ bone marrow cells from mice treated with Ctrl and BTZ. ΔCtrl and ΔBTZ were calculated to remove non-specific staining (Δ = $p53^+$ frequency - $isotype^+$ frequencies). Note: 0.004% of $CD45^+$ cells in Ctrl mice and 0.85% of $CD45^+$ cells in BTZ treated mice positive for p53, whereas 99.99%, and 99.15% $CD45^+$ cells in Ctrl and BTZ treated mice are p53 negative. (*F*) Duplex mRNA ISH analysis of *Trp53/Kit* in the bone marrow of p53 wild-type mice. Scale bars, 20 μm.

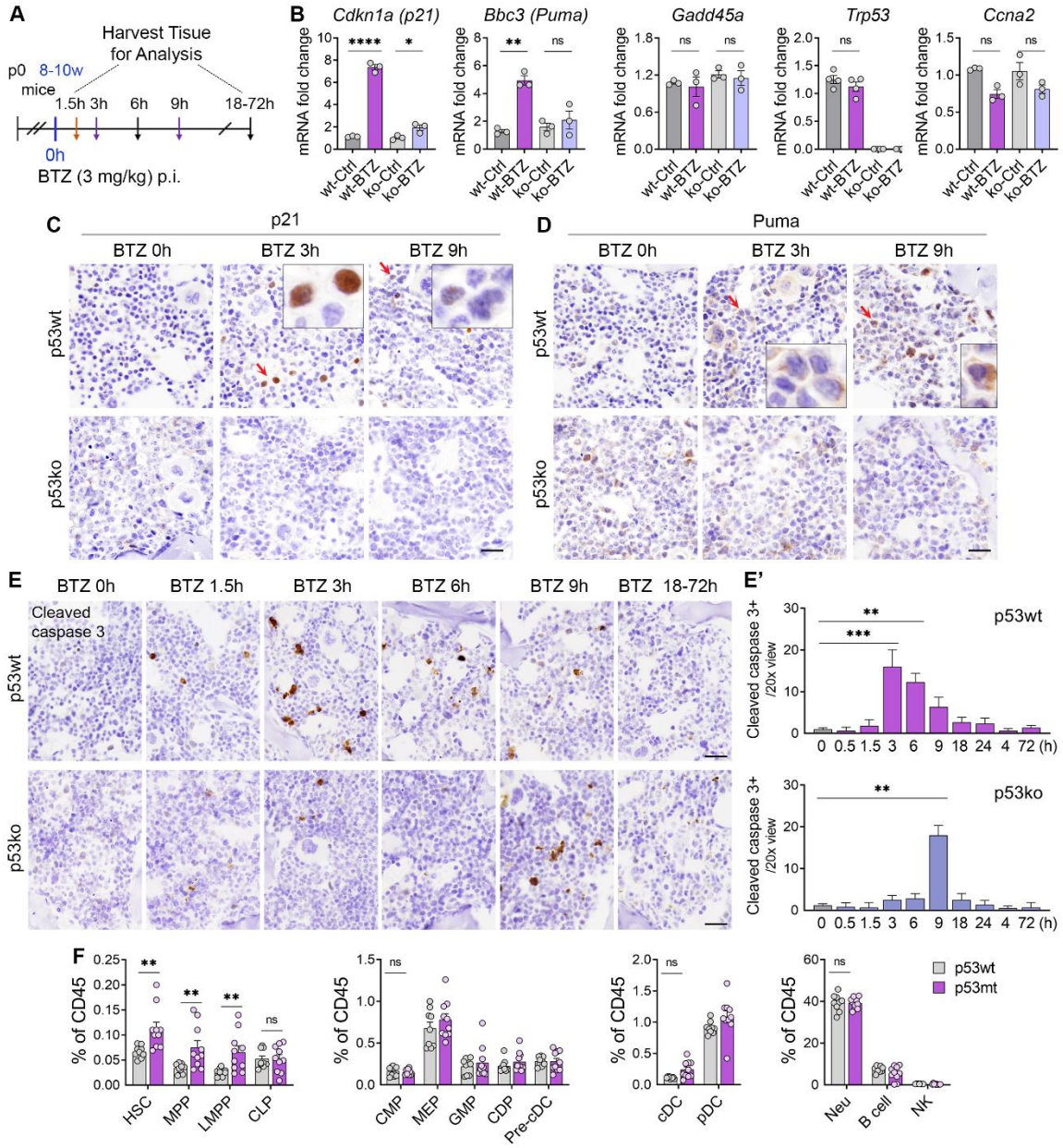

Fig. 3. p53 target gene expression and apoptosis induction in bone marrow following bortezomib treatment. (*A*) The schedule of bortezomib (BTZ) experiments for detecting p53 target gene and apoptotic induction (n = 3-4). p0, neonatal; w, week, h, hour; p.i., intraperitoneal injection. (*B*) qPCR analysis of *Cdkn1a, Puma*, *Gadd45a*, *Trp53*, and *Ccna2* expression in the bone marrow of p53wt and p53ko mice treated with BTZ (3 mg/kg, 3h). (*C* & *D*) IHC analysis of p21 and Puma in the bone marrow from mice at indicated time points post vehicle (BTZ 0h) or 3 mg/kg BTZ treatment. Scale bars, 20 μm. (*E* & *E'*) IHC analysis and quantification of the expression of cleaved caspase 3 in the bone marrow of $p53^{+/+}$ and $p53^{-/-}$ mice at indicated time points post vehicle (BTZ 0h) or 3 mg/kg BTZ treatment (n = 3-4). Scale bars, 20 μm. (*F*) Quantification of the frequencies of HSPCs and various mature cells in the bone marrow from p53wt and p53mt mice (n = 9-10). For B, the indicated P values were calculated by two-way ANOVA using Prism. For C' and D, the indicated *p* values were calculated using multiple unpaired t-tests using Prism. *, $P < 0.05$; **, $P < 0.001$; ***, $P < 0.0001$; ****, $P < 0.00001$, ns, no significance. The error bars represent the Mean (SEM) for each group.

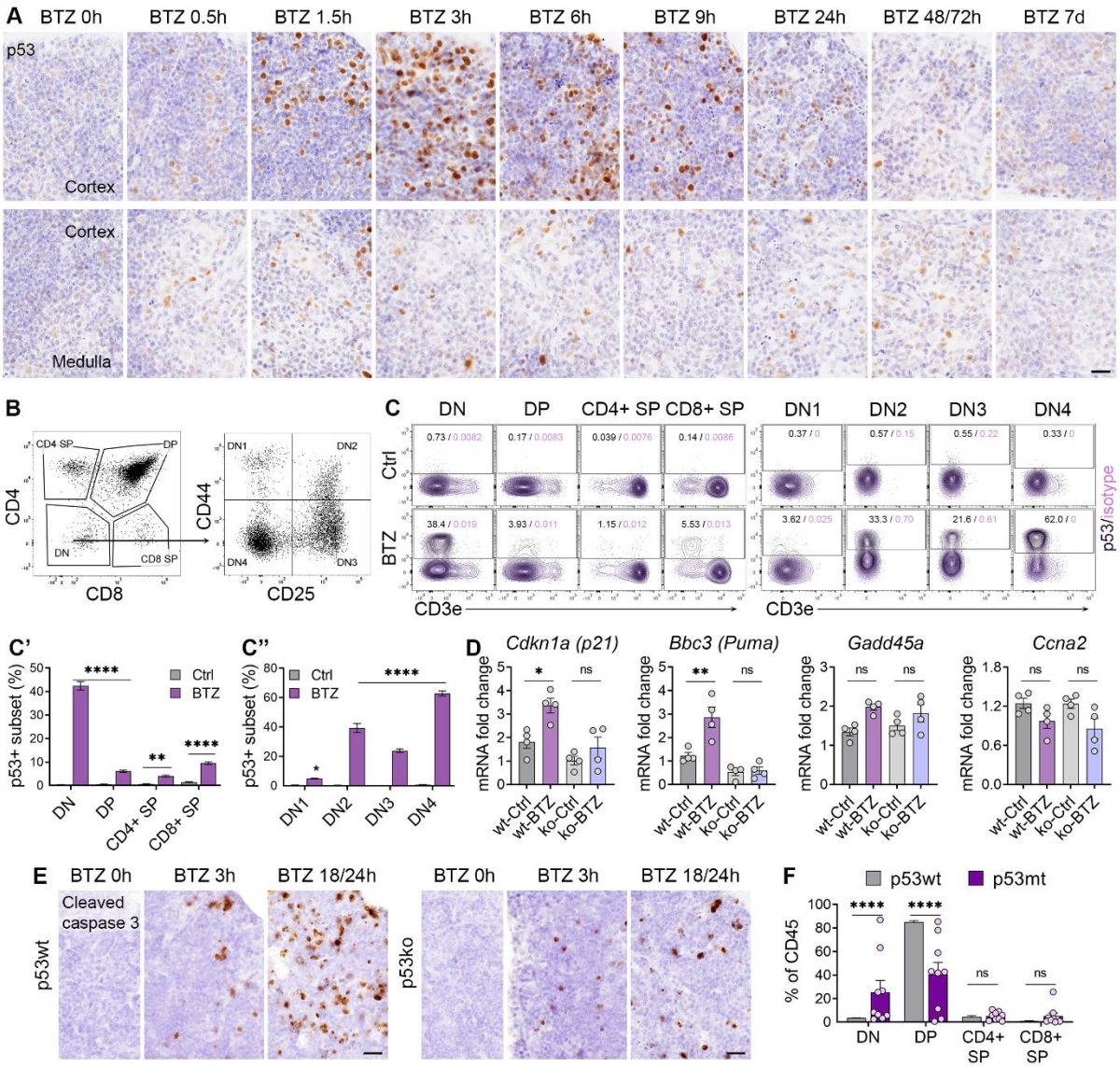

Fig. 4. Stabilization of p53 in the thymus by bortezomib. (*A*) IHC analysis of p53 levels in the thymus from mice at indicated time points post vehicle or 3 mg/kg BTZ treatment. Upper panel: thymus cortex, bottom panel: thymus medulla or medulla/cortex region (n = 3-4). Scale bars, 20 µm. (*B*) Gating strategy for analyzing thymocytes based on expression of CD4 and CD8, and DN subsets based on expression of CD44 and CD25. (*C*) Representative FACS plots of p53-positive subsets in various T cell development stages and the DN subsets. (*C'* & *C"*) Quantification of the frequency of $p53^{+}$ subsets in respective parent cell populations. (*D*) qPCR analysis of *Cdkn1a, Puma*, *Gadd45a*, *Trp53*, and *Ccna2* expression in the thymus of $p53^{+/+}$ and $p53^{-/-}$ mice treated with BTZ (3 mg/kg, 3h). (*E*) IHC analysis of the expression of cleaved caspase 3 in the thymus of $p53^{+/+}$ and $p53^{-/-}$ mice at indicated time points post vehicle (BTZ 0h) or 3 mg/kg BTZ treatment (n = 3-4). Scale bars, 20 µm. (*F*) Quantification of the frequencies of various T cell subsets in the thymus from p53wt and p53mt mice (n = 7-9). For C', C'' and F, the indicated *p* values were calculated by multiple unpaired t-tests of using Prism; For D, the indicated P values were calculated by two-way ANOVA using Prism; *, P < 0.05; **, P < 0.001; ***, *P* < 0.0001; ****, P < 0.00001; ns, no significance. Error bars, mean (SEM) for each group.

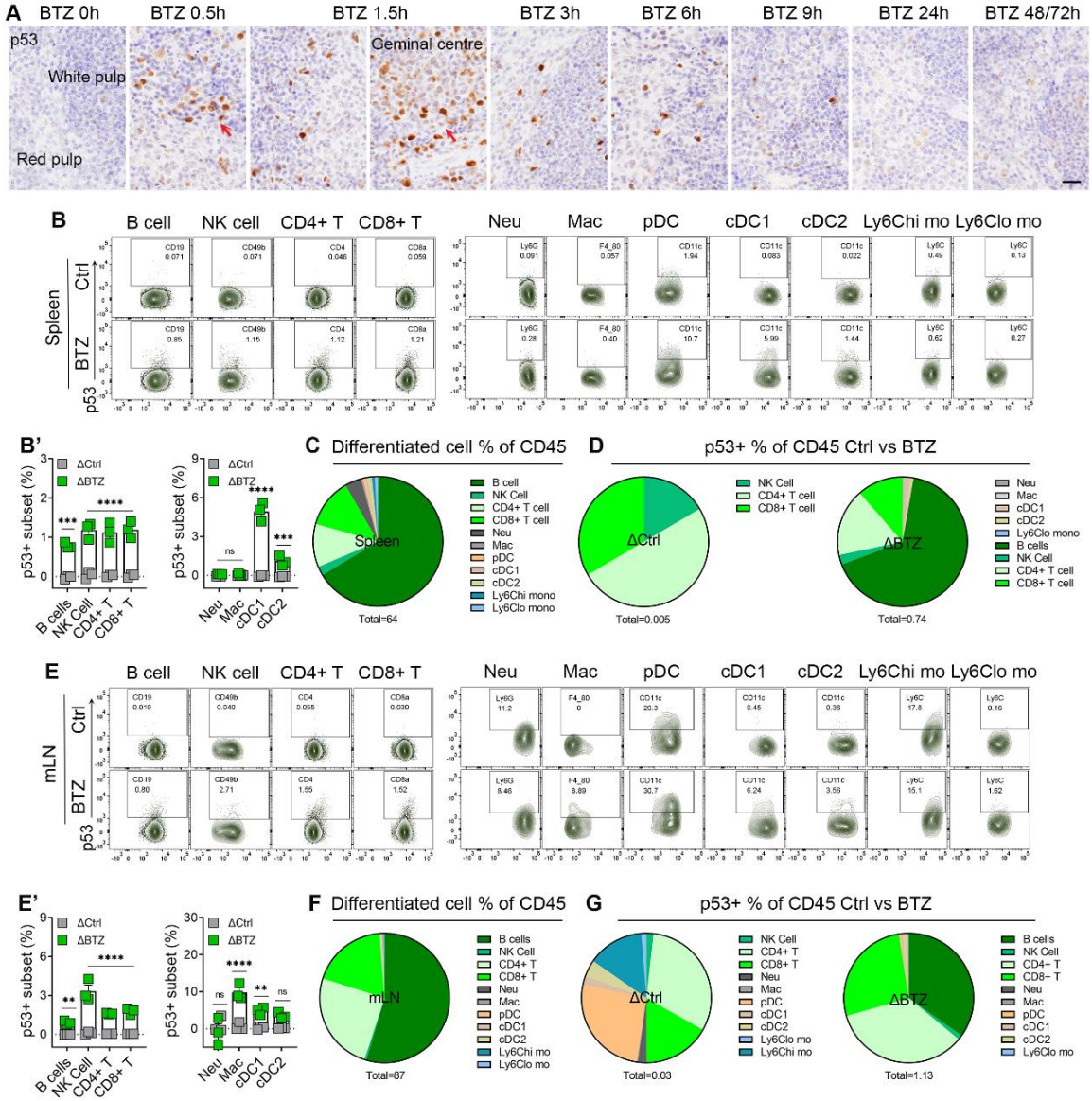

Fig. 5. Stabilization of p53 in the spleen and lymph node by bortezomib. (*A*) IHC analysis of p53 levels in the spleen from mice at indicated time points post vehicle control (Ctrl, BTZ 0h) or 3 mg/kg BTZ treatment. Red arrows point to the germinal centre. Scale bars, 20 µm. (*B*) Representative FACS plots showing the splenocytes stained for p53 from mice treated with Ctrl or BTZ for 1.5h, gated on matured lymphoid and myeloid cells. (*B'*) Quantification of p53$^+$ subsets of the indicated splenocytes from mice treated with Ctrl (in grey) or BTZ (in green). (*C*) Quantification of frequencies of various splenocytes of CD45$^+$ cells from mice treated with Ctrl. 64% of the total CD45$^+$ population was analyzed. (*D*) Quantification of frequencies of p53$^+$ in splenocytes of CD45$^+$ cells from mice treated with Ctrl and BTZ. ΔCtrl and ΔBTZ were calculated to exclude non-specific staining (Δ = p53$^+$ frequency - isotype$^+$ frequencies). (*E*) Representative FACS plots showing staining for p53 in mLN cells from mice treated with Ctrl or BTZ for 1.5h, gated on matured lymphoid and myeloid cells. (*E'*) Quantification of p53$^+$ subsets of the indicated mLN cells from mice treated with Ctrl (in grey) or BTZ (in green). (*F*) Quantification of the frequencies of various CD45$^+$ mLN cells from mice treated with Ctrl. A total of 87 CD45$^+$ cells were analyzed. (*G*) Quantification of frequencies of p53$^+$ in mLN cells of CD45$^+$ cells from mice treated with Ctrl and BTZ. ΔCtrl and ΔBTZ were calculated to exclude non-specific staining (Δ = p53$^+$ frequency - isotype$^+$ frequencies). For A-G, n = 3-4. For B' and E', the indicated *p* values were calculated by multiple unpaired t-tests using Prism. **, $P < 0.001$; ***, $P < 0.0001$; ****, $P < 0.0001$; ns, no significance. The error bars represent the Mean (SEM) for each group.